Deep Flow along the Western Boundary South of the Blake Bahama Outer Ridge

ELIZABETH JOHNS

National Oceanic and Atmospheric Administration, Atlantic Oceanographic and Meteorological Laboratory, Miami, Florida

RANA A. FINE

University of Miami, Rosenstiel School of Marine and Atmospheric Science, Miami, Florida

ROBERT L. MOLINARI

National Oceanic and Atmospheric Administration, Atlantic Oceanographic and Meteorological Laboratory, Miami, Florida

(Manuscript received 14 July 1995, in final form 7 April 1997)

ABSTRACT

In June–July 1990, hydrographic, chlorofluorocarbon (CFC), and velocity observations were taken along the western boundary of the North Atlantic south of the Blake Bahama Outer Ridge from 30° to 24°N between the northern Bahamas and 71°W. The deep flow in the region, associated with the deep western boundary current, forms a pattern of strong, narrow currents and cyclonic gyres close to the continental slope with broad, slower southward flow offshore. The CFCs reveal that the most recently ''ventilated'' water (i.e., having the highest CFC concentrations due to more recent contact with the atmosphere in the northern North Atlantic) is found along the western boundary in two distinct cores between potential temperatures 4°–6°C and 1.9°–2.4°C. Geostrophic transport streamlines were constructed for the deep flow, referenced using direct velocity observations at 26.5°N and assuming mass conservation between closed areas bounded by the hydrographic sections. The tracers and transports are used together to describe the deep circulation in the region, to determine the origins and pathways of the various flow components, to define the spatial scales and strengths of the deep currents and recirculation gyres, and to examine their relationship to bottom topography and their possible role in ventilating the interior. The close correspondence of the tracer distributions with the regional bottom topography implies that the major topographic features in this region strongly influence the deep circulation. The geostrophic transport for the narrow branch of current having the highest CFC concentration, which transits the region and continues equatorward adjacent to the western boundary, is 31 Sv (Sv $\equiv 10^6$ m^3 s^{-1}) below 6°C. A cyclonic gyre with one or more embedded gyres extends offshore of the narrow boundary current out to about 74°W, transporting 12 Sv of water with intermediate CFC concentrations. Farther offshore, a broad band of southward flow contributes an additional 16 Sv of water with considerably lower CFC concentrations. Thus there is a total deep (<6°C) equatorward transport through the study area along the western boundary of 47 Sv at 24°N. The layer containing the shallower CFC core (4°–6°C) appears to be less constrained by the bottom topography. Within this temperature layer, one current branch with high CFC and low salinity flows southward along the Blake Escarpment. However, there is another branch of flow within this layer that forms an extended zonal high CFC and high salinity distribution from the eastern to the western bounds of the study region. This second branch apparently originates in the Gulf Stream recirculation and carries the higher salinity influence of the Mediterranean Water.

1. Introduction

As a major component of the global thermohaline circulation, the deep western boundary current (DWBC) in the North Atlantic carries recently ventilated waters equatorward. The flow is strongly constrained by the bottom topography, with the most recently ventilated water located for the most part adjacent to the steepest part of the continental slope. However, some portion of the recently ventilated deep water also extends into the interior due to mixing and advection in recirculation gyres (e.g., Hogg et al. 1986). Herein, data collected in the western subtropical North Atlantic during June–July 1990 are used to show that the path of the DWBC through this region is complex and includes recirculation gyres with spatial scales ranging from a few hundred kilometers to nearly basin scale.

The study region lies east of the northern Bahamas, between the Blake Bahama Outer Ridge (BBOR) at 30°N and the San Salvador Spur at 24°N (Fig. 1). The region is characterized by complicated bottom topography with a steep continental slope, ridges, and valleys,

Corresponding author address: Dr. Elizabeth Johns, NOAA/AOML, 4301 Rickenbacker Causeway, Miami, FL 33149.
E-mail: johns@aoml.noaa.gov

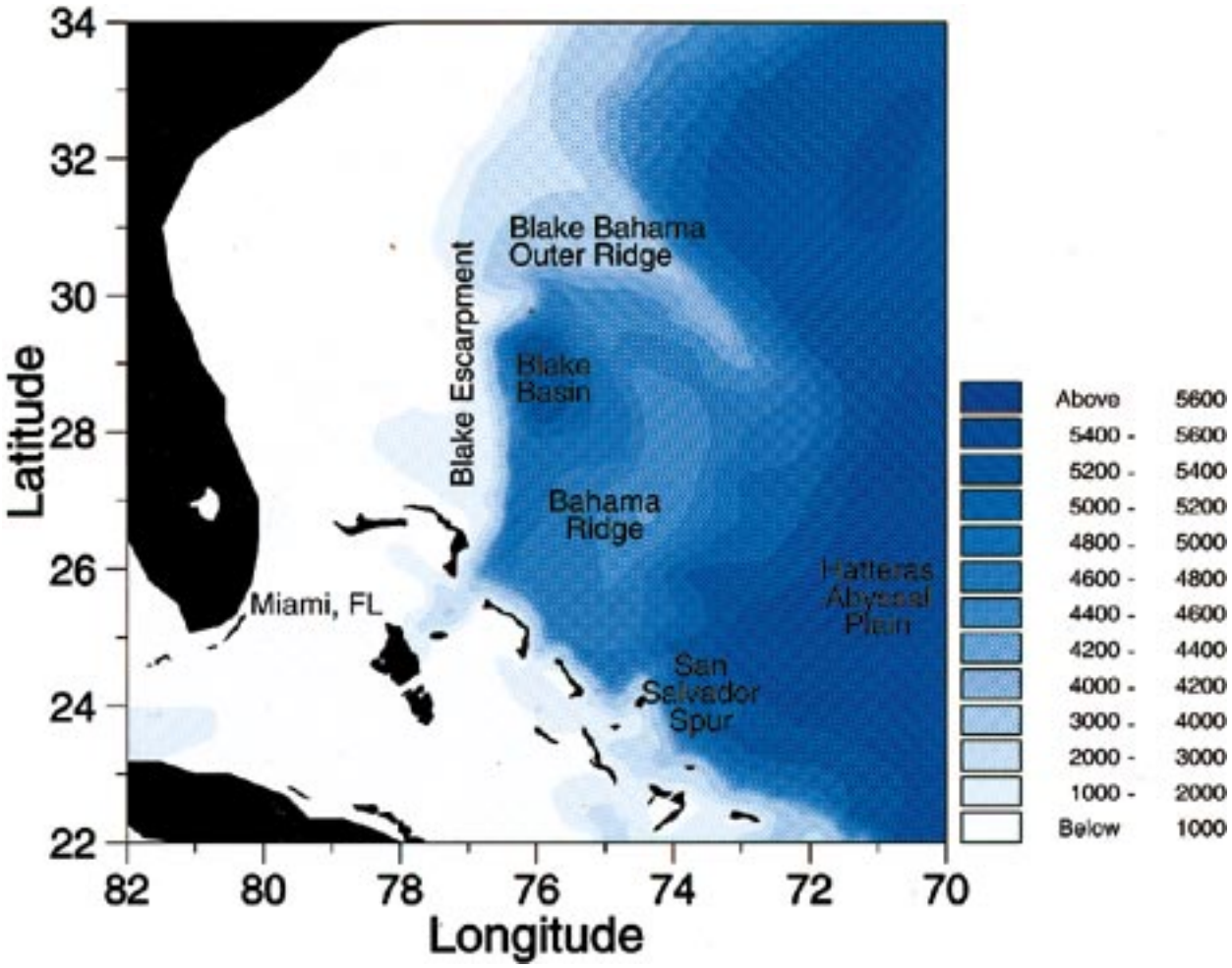

FIG. 1. Bottom topography (m) in the western North Atlantic Ocean in the vicinity of the Blake Bahama Outer Ridge.

and dramatic changes in direction of the bottom depth gradients. All of these factors can be expected to have a significant role in steering the deep flow. The predominant feature of the regional bottom topography is the BBOR, where depths shallower than 4600 m extend to the southeast from the western boundary several hundred kilometers into the Hatteras Abyssal Plain. The axis of the BBOR recurves back to the southwest and connects to a secondary ridge, the Bahama Ridge (Fig. 1). The Blake Basin, where depths exceed 5400 m, is located between the Blake Escarpment and the BBOR. Farther to the south (near 24°–25°N), the San Salvador Spur is located near the southern limit of the Bahama Ridge, which appears to be an important factor in steering the deep flow.

Several distinct water masses are contained within the DWBC in the study region. These water masses have been identified and differentiated by their tracer signatures (cf. the review article by Fine 1995). Below 6°C, chlorofluorocarbon (CFC) tracers have the highest concentrations in two ''cores'' located adjacent to the continental slope (Fine and Molinari 1988; Smethie 1993; Watts 1991). The shallow layer between 4° and 6°C is believed to have formed in the southern Labrador Sea (Pickart 1992) and is called Shallow Labrador Sea Water (SLSW). The SLSW is less dense than ''classical'' Labrador Sea Water (Talley and McCartney 1982). Below the SLSW, there is a tracer minimum at potential temperatures representative of LSW and Iceland–Scotland overflow water (Swift 1984). LSW is formed sporadically over a decadal timescale and did not show as a tracer maximum south of the Grand Banks at the time of the June–July 1990 survey. The deep tracer maximum between 2.4° and 1.9°C is a combination of Gibbs Fracture Zone water and Denmark Strait overflow water (DSOW), which will be called overflow water (OW). The DSOW is the primary contributor of the transient tracer signal to the deeper core (Livingston et al. 1985; Smethie and Swift 1989; Smethie 1993). Below the deep core lies another layer that is low in tracer concentration, comprising a mixture of OW and recirculating Antarctic Bottom Water (e.g., Amos et al. 1971; McCartney and

Talley 1984; Schmitz and McCartney 1993; Baringer et al., manuscript in preparation[1]; McCartney and Curry 1996).

A number of earlier studies portray strong deep currents in the region and illustrate possible topographic steering of these flows. Bottom photographs in the western North Atlantic indicate that there are ''geostrophic contour-following bottom currents,'' which parallel the isobaths of the continental margin (e.g., Heezen et al. 1966; Hollister and Heezen 1972; Tucholke et al. 1973). Tucholke et al. (1973) provide a summary of bottom photographic results and direct current measurements of the deep flow in the region. These observations show deep equatorward flow on the eastern flank of the BBOR, which then turns westward toward the continental slope and flows southward along the Blake Escarpment. Northward flow offshore on the eastern rim of the Blake Basin forms a small cyclonic recirculation gyre. Farther to the southeast, near 25°–26°N, 72°–73°W, there is southward flow. In addition to these indications from bottom photographs, the use of sediment type as a tracer of the bottom water circulation also suggests that the deep flow through the region tends to be parallel to the isobaths and gives indications of gyrelike recirculations (Tucholke et al. 1973).

Using hydrographic data collected across the BBOR in 1968 at approximately 30°N, Amos et al. (1971) found that the southeast orientation of the BBOR diverted part of the DWBC flow away from the western boundary. They also found that the deep flow then turned around the tip of the BBOR to flow westward to the Blake Escarpment before flowing equatorward again. The highest bottom velocities were observed on the eastern flank of the BBOR and at the Blake Escarpment. They inferred a cyclonic circulation pattern around the Blake Basin similar to that of Tucholke et al. (1973).

Lagrangian float observations provide a dramatic example of the temporal and spatial variability of the flow in this region, much of which appears to be closely related to the regional bottom topography. Between 1973 and 1976 Riser et al. (1978) deployed SOFAR floats at depth 1500–2000 m in the region of the BBOR. Three of the floats were caught in the DWBC along the Blake Escarpment (their Figs. 2, 3, and 5). One float crossed southwestward over the BBOR north of 30°N and then was transported cyclonically around the Blake Basin. The other two floats also crossed the BBOR near 30°N in a small (diameter ~20 km) eddy, then upon reaching the Blake Escarpment moved rapidly southward to about 25°N. At this point, the float that was farther offshore was deflected northward, while the other followed the topographic contours around the San Salvador Spur past 24°N and continued equatorward along the boundary.

An intensive study of the DWBC in the Atlantic east of Abaco Island, the Bahamas, at 26.5°N was conducted as part of NOAA's Subtropical Atlantic Climate Study (Molinari 1989; Rosenfeld et al. 1989; Leaman and Harris 1990; Lee et al. 1990). This program, which used hydrographic and direct velocity measurements from acoustic velocity profilers and moored current meters, yielded a mean deep (>800 m) equatorward volume transport estimate of 33 Sv (Sv $\equiv 10^6$ m^3 s^{-1}) for the portion of the western boundary between Abaco Island and about 75°W (Lee et al. 1990). This transport was considerably larger than had been expected at this latitude. Lee et al. (1990) speculated that there might be a deep cyclonic gyre trapped over the Bahama Ridge and that southward flow associated with the inshore side of the gyre (the only part sampled by the current meter array) contributed to the unexpectedly high transport at 26.5°N. On a larger scale, Schmitz and McCartney (1993) portray an elongated cyclonic gyre with a transport of 17 Sv in the western basin just offshore of the DWBC, extending from the equator to about 30°N. They propose that the transport associated with this gyre may add to the 17 Sv of DWBC transport from northern sources, to give a combined equatorward western boundary transport of 34 Sv south of 30°N.

Transient tracer observations in this region were taken in 1977 by Jenkins and Rhines (1980) who occupied a hydrographic section across the BBOR. They observed a plume of high tritium with maximum concentration located at a potential temperature of 1.9°C. The plume was tightly confined to the bottom at the ridge crest and was intensified on the eastern flank of the ridge. Current meter data collected in the vicinity of the plume as part of the same study (Mills and Rhines 1979) showed bottom-intensified southeastward flow, parallel to the isobaths, with an average velocity of 20 cm s^{-1}. West of the BBOR crest, the flow was westward toward the Blake Escarpment and then turned southward along the boundary. Farther south, near 26°N, Olson et al. (1986) observed a several hundred kilometer wide tritium core with highest concentration adjacent to the continental slope. This is in contrast to the much narrower (~50 km) tritium core observed farther north at the BBOR by Jenkins and Rhines (1980).

These previous studies all demonstrate the complexity of the path of the DWBC through the region and its relationship to local bottom topographic features. Herein, hydrographic, direct velocity, and chloroflourocarbon (CFC) data collected during June–July 1990 are used to quantify and map the three-dimensional characteristics of the DWBC and its recirculation gyres between the BBOR and 24°N. A description of the dataset is followed by a discussion of the methodology used to estimate geostrophic velocity and transport from the hydrographic section data and direct velocity observations. The interaction between the boundary and the interior

[1] Bottom water circulation in the subtropical western Atlantic observed during the August 1992 Trident Expedition.

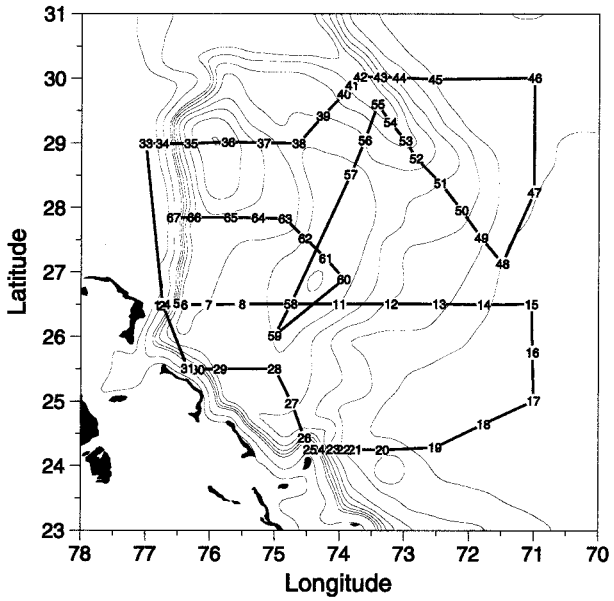

FIG. 2. Cruise track and CTD station locations for the June–July 1990 cruise aboard the NOAA Research Vessel *Malcolm Baldrige.*

is described from tracer and flow fields within several temperature layers using vertical sections and horizontal maps. The discussion focuses on the large-scale pathways of the DWBC flow, the relationship of the deep flow to the bottom topography, the influence of the Gulf Stream on the tracer and flow fields in the upper layer of the deep flow, and the role of the recirculation gyres in the ventilation of the interior and the equatorward dilution of the DWBC tracer concentrations.

2. Data

The CTD and tracer data were collected during the period 18 June–9 July 1990 aboard the NOAA Research Vessel *Malcolm Baldrige* at station locations shown in Fig. 2. The first leg of the cruise (CTD stations 1–32) covered the southern half of the study region, including transects between 26.5°N and the San Salvador Spur at 24°N. The second leg (CTD stations 33–67) covered the northern half of the study region, including transects east of the BBOR at 30°N, along the axis of the BBOR and western boundary transects at 29° and 28°N.

The CTD data were collected using a Neil Brown Mark III system, which included pressure, temperature, and conductivity sensors. Data processing and calibration details are given in Johns and Wilburn (1993). Pressure accuracy is approximately ±3.0 db and temperature accuracy is ±0.005°C, based on pre- and postcruise laboratory calibrations. Bottle salinities were collected using a 24-bottle rosette sampler lowered with the CTD and analyzed on a Guildline Autosal unit inside a temperature-controlled van. The bottle salinities were accurate to ±0.002 (PSS-78) based on autosal standard sample readings and comparison of duplicate samples, and were used to check the laboratory calibration of the CTD conductivity sensor. Some drift of the conductivity sensor occurred, resulting in a mean offset between bottle and laboratory-calibrated CTD salinity values that ranged from −0.005 to +0.006 over the course of the cruise. This drift was accounted for in the final calibration, yielding a CTD salinity dataset with a standard deviation from the bottle salinities of ±0.002 for the entire cruise.

Samples for analysis of CFCs (CFC-11 and CFC-12) were collected and analyzed at sea using an analytical system similar to that of Bullister and Weiss (1988). Bottle and handling blanks were estimated by rotating and double tripping the bottles and comparing to data at nearby stations. Due to a high blank the CFC-12 data are not used here. A bottle blank of 0.003 pmol kg^{-1} was applied for CFC-11. The analytical blanks for CFC-11 ranged from 0.000 to 0.027 pmol kg^{-1} with an average of 0.002 pmol kg^{-1}. The average standard deviation of a series of replicates taken from duplicate syringes drawn on the same bottle for CFC-11 was ±0.004 pmol kg^{-1} (or 1% relative standard deviation) for concentrations >0.100 pmol kg^{-1}, and 0.002 pmol kg^{-1} for concentrations <0.100 pmol kg^{-1}.

Estimates of total water column transport were obtained using depth-averaged velocities from moored current meters and dropsondes along 26.5°N to reference geostrophic velocity profiles computed from the CTD data. Measurement uncertainty in the current meter velocities is on the order of ±1 cm s^{-1} (R. Zantopp 1994, personal communication). The deployment and surfacing locations of the dropsondes were obtained using LORAN C navigation. Uncertainties in dropsonde depth-averaged velocity are on the order of ±2 cm s^{-1} based on comparisons with collocated Pegasus acoustic velocity profiler casts taken on other cruises (M. Bushnell 1994, personal communication).

3. Geostrophic velocity referencing methodology

a. Geostrophic velocity referencing along the 26.5°N transect

Directly observed velocities were available from an array of current meters moored along the 26.5°N transect (Lee et al. 1990). Mean velocities computed from the current meters (12-h averaged, 40-h lowpass filtered) for the period 18–25 June 1990, while the 26.5°N CTD transect was being occupied, were used for the analysis. Vertical profiles from the current meter array are shown in Fig. 3. The most western or onshore mooring, CM 268, shows shallow southward flow of −20 cm s^{-1} with an underlying core of northward flow centered at about 400 m. The CM 270 mooring is located in the core of the DWBC, showing a middepth southward maximum velocity of −22 cm s^{-1} at 2000-m depth. The two current meters bracketing this core, CM 269 and CM 271, both show weaker southward flow over the entire water

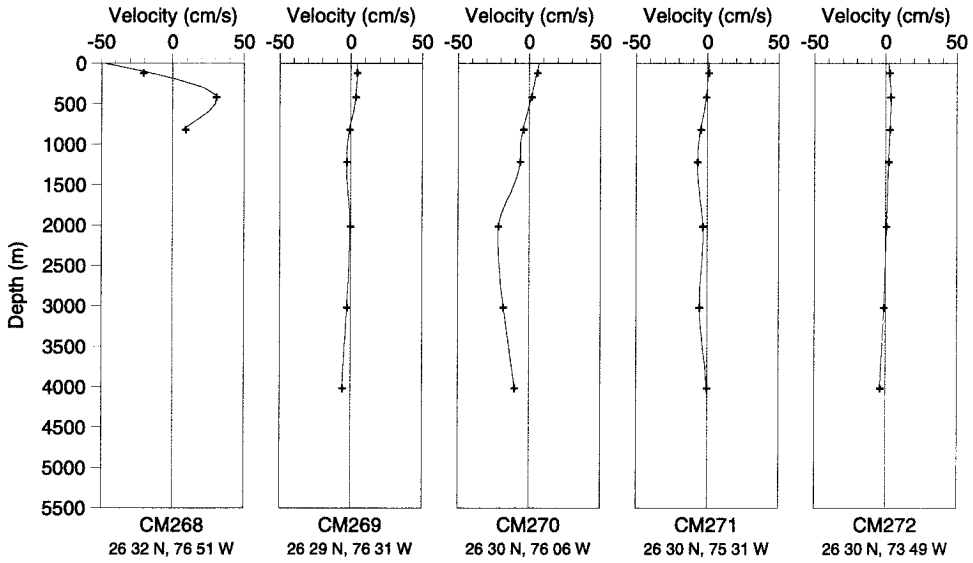

FIG. 3. Northward velocity profiles (cm s^{-1}) along 26.5°N from moored current meter data averaged over the time period 18–25 June 1990.

column below 800 m. The most eastern, or offshore, current meter mooring, CM 272, shows almost no flow at all with weak southward flow near the bottom.

Geostrophic velocity profiles were computed along 26.5°N between pairs of adjacent CTD casts using standard methodology. The profiles were initially referenced relative to zero velocity at the greatest common depth of each pair, in most cases within tens of meters of the bottom. Comparison of the geostrophic velocity profiles (referenced as described below) with the vertical structure of the current meter data, interpolated laterally to the locations of the midpoints of the CTD pairs used to generate each geostrophic profile (Fig. 4), shows that they are very similar in shape and indicates that the flow must therefore be predominantly geostrophic. The exception to the good agreement of shears is for CTD pairs 8–58 and 58–11, where the current meter horizontal spacing failed to resolve an upper-layer eddy. The deep shear structures of the geostrophic velocity profiles and the bracketing current meters, however, are in close agreement.

In addition to the current meter moorings, several dropsondes (which yield a single average water column velocity value at each deployment location) were also taken along 26.5°N at about 74.5°W near the top of the Bahama Ridge, near 74°W, and farther offshore at about 72.5°W (Fig. 2). Average water column velocities from the dropsondes were used to reference the geostrophic velocity profiles where the horizontal spacing of the current meter array did not fully resolve important features of the velocity field, for example, between CTD pairs 8–58 and 58–11 in the eddy discussed in the previous paragraph.

Depth-averaged (whole water column) velocities from the current meter array and the three dropsondes were used to reference the geostrophic velocity profiles. The depth-averaged velocities from the current meter moorings, the dropsondes, and the referenced geostrophic velocity profiles are shown versus distance from 77°W along 26.5°N in Fig. 5. Depth-averaged flow is to the north just inshore of the strongest southward flow. The equatorward flow reaches a maximum of −12 cm s^{-1} at about 90 km from the boundary. The dropsonde taken near the crest of the Bahama Ridge (near 220 km) shows that the depth-averaged flow is to the north there. The dropsonde located farthest to the east, at about 450 km, showed a return to southward depth-averaged flow. The difference between the depth-averaged geostrophic velocity and the depth-averaged direct (current meter and/or dropsonde) velocity interpolated to the CTD pair midpoint location provided the reference velocity (or bottom velocity in this case) needed to adjust the geostrophic profiles along 26.5°N. East of the last dropsonde, in the absence of any other direct velocity information, it was assumed that the flow at the bottom was zero. The resulting referenced geostrophic velocity section is shown in Fig. 6. The deep flow below approximately 800 m shows two southward branches with the stronger, narrower branch located near the western boundary at about 90 km and a wider, weaker branch farther offshore. These two branches of current are separated by northward flow centered over the Bahama Ridge.

b. Geostrophic velocity referencing away from the 26.5°N transect

In order to determine reasonable bottom velocities for the geostrophic flow away from the 26.5°N section, where direct velocity information was not available,

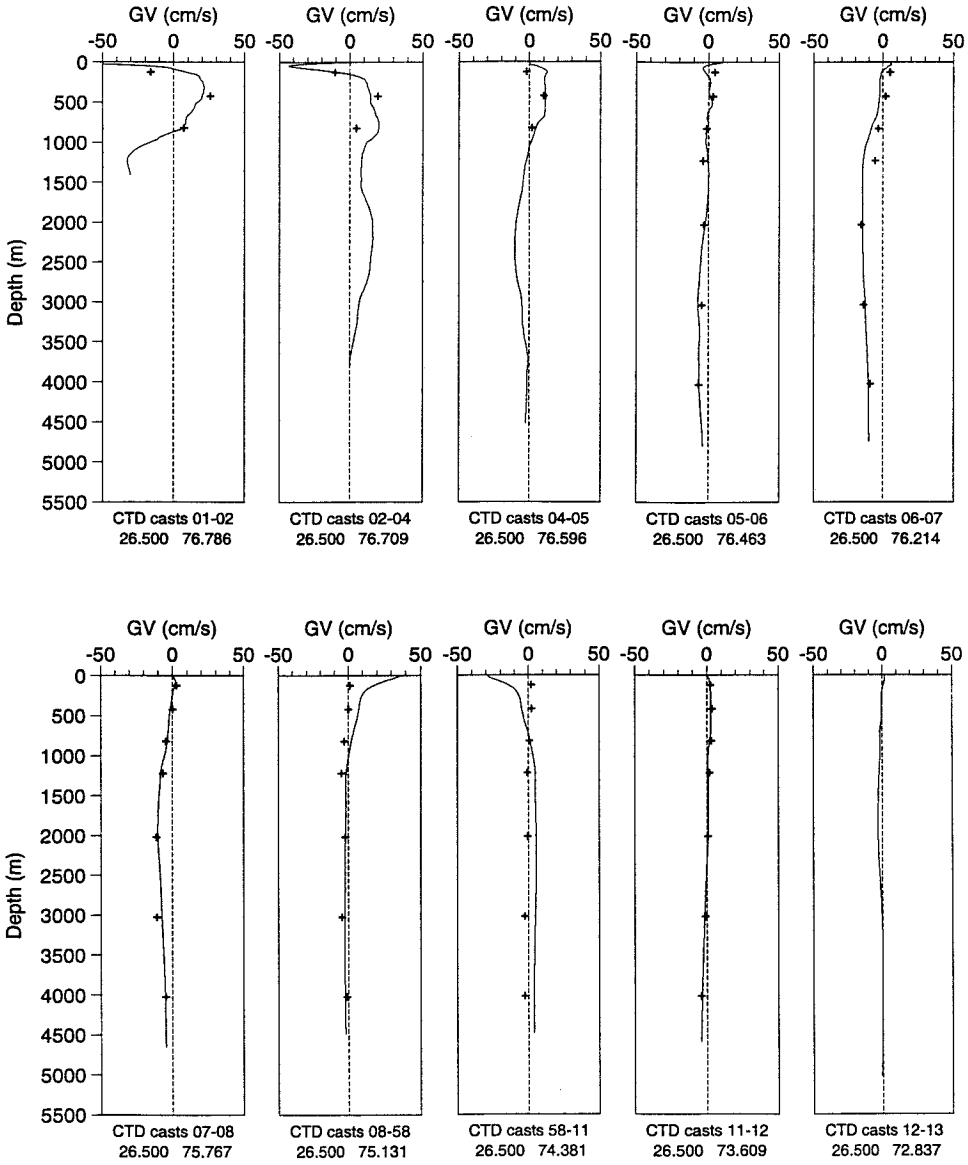

FIG. 4. Geostrophic velocity profiles from pairs of CTDs along 26.5°N, with current meter velocities (+) horizontally interpolated to the CTD pair midpoints from bracketing current meter moorings.

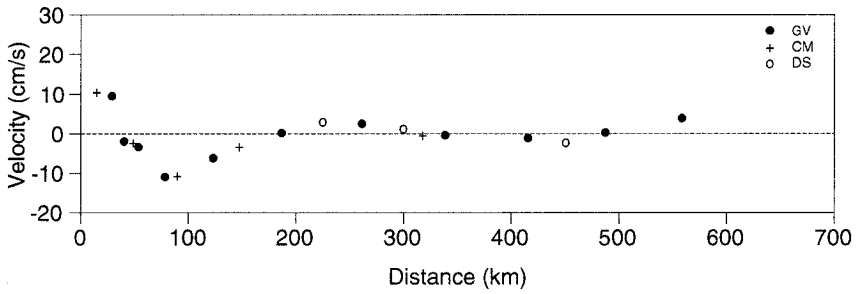

FIG. 5. Northward depth-averaged geostrophic, current meter, and dropsonde velocity (cm s^{-1}) along 26.5°N used for computation of reference velocity.

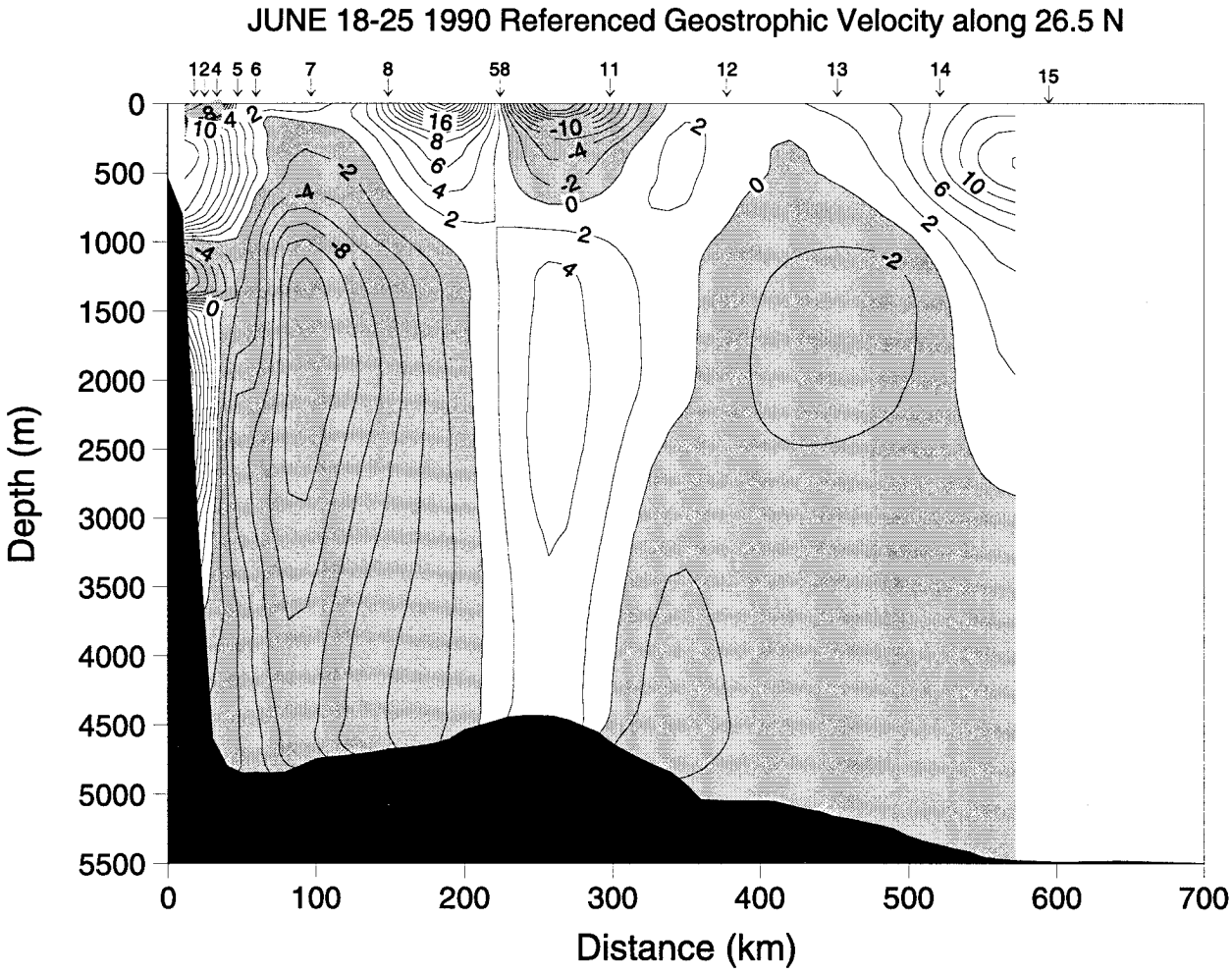

FIG. 6. Northward referenced geostrophic velocity section (cm s^{-1}) along 26.5°N.

several assumptions and constraints were used. The general philosophy follows that used by Reid (1994) to infer reference velocities and large-scale flow patterns in the North Atlantic, with the goal being to find the simplest portrayal of the circulation in which the transport balances (i.e., mass is conserved) and the flow field is consistent with the tracer distributions.

The cruise track was divided into closed boxes formed by subgroups of CTD stations. The sections were divided in the vertical into four potential temperature layers (4°–6°, 2.4°–4°, 1.9°–2.4°, and ≤1.9°C) chosen on the basis of the CFC-11 distributions to best delineate the different core water masses of the region. Within each box it was assumed that total transport should be balanced in the deep water (<6°C). The tracer distributions were examined within the chosen temperature intervals, and the large-scale flow was expected to be consistent with the tracer patterns. In addition, unless otherwise dictated by the tracer distributions and mass balances, the flow was assumed to be aligned primarily along rather than across contours of bottom depth.

The next step was to determine the magnitude and direction of the minimum reference velocity for each CTD station pair that would best satisfy the assumptions and constraints. In this way a pattern of reference velocity was generated, corresponding to the deepest velocities shown in the velocity sections of Figs. 7–10. Once the reference, or bottom, velocity field was established, referenced geostrophic velocity sections were generated (Figs. 7–10), and vector maps representing the balanced flow field for the total deep water and in the various isotherm layers were produced (Figs. 11, 12, 14, 16, and 17). The total deep (<6°C) transport balances over the domain to within 1 Sv. However, individual sublayers showed imbalances in a few cases of up to 2–3 Sv. There are several possible reasons for these errors, most important of which is probably the lack of synopticity of the dataset, which was collected over a period of three weeks. Lee et al. (1996), using direct current meter velocity observations obtained along 26.5°N, find very energetic signals with a 100-day period.

The availability of direct velocities along 26.5°N provided a strong constraint on the reference velocity pattern. Nevertheless, it must be emphasized that the resulting flow maps are transport balancing schematics and not direct observations. Away from 26.5°N, there is increasing ambiguity in the streamline patterns as there is more than one way to conserve the transport in each box, and tracer distributions and bottom topography in these areas provided an increasingly important constraint on the inferred circulation. Nevertheless, the transport balance errors and ambiguities in the flow patterns are significantly smaller than the calculated total transports, and only small changes can be made to the estimated bottom velocities and computed referenced geostrophic transports without causing inconsistencies with the tracer fields or large imbalances in the total transport through the observational domain.

4. Vertical sections

Vertical sections show the layered structure of the tracer concentrations and their location relative to the velocity structure of the water column and will be described before presenting the transport streamlines and tracer maps. This discussion centers on the four primarily zonal sections (29°–30°N, 28°N, 26.5°N, and 25.5°–24°N) of Figs. 7 through 10.

The northernmost transect begins at 29°N along the Blake Escarpment, angles up to the northeast over the western slope of the BBOR, and then turns to the east along 30°N on the eastern slope of the BBOR and out into the deep waters of the Hatteras Abyssal Plain (Fig. 7, upper panel). The geostrophic velocity section (Fig. 7, middle panel) shows bottom-intensified southward flow along the eastern BBOR flank at 30°N (CTD stations 44–45) similar to that observed by Amos et al. (1971) and Mills and Rhines (1979). The deep flow is northwestward on the western flank of the BBOR (stations 37–42) and then strongly southward along the continental slope at 29°N (stations 34–36). Along the boundary at 29°N a southward velocity core with a middepth (~2500 m) maximum is observed.

Highest CFC-11 concentrations along the 29°–30°N transect (Fig. 7, lower panel) are located within an elongated layer centered at 4.4°C, which extends over the length of the section out to at least 71°W. These high CFC-11 concentrations are characteristic of the SLSW core described previously. Within the deeper ventilated layer (1.9°–2.4°C), the highest CFC-11 concentrations are found in two cores, one over the deepest part of the Blake Basin and the other along the eastern flank of the BBOR crest.

The 28°N transect extends across the Blake Escarpment along the southern edge of the Blake Basin, then angles toward the southeast to join the 26.5°N transect at about 74°W (Fig. 8, upper panel). The velocity section (Fig. 8, middle panel) shows a nearly identical DWBC structure adjacent to the steep continental slope of the Blake Escarpment as that at 29°N, with a velocity maximum centered at about 2500 m and similar current widths. Approximately 300 km offshore there is northeastward flow over the Bahama Ridge.

The upper (4°–6°C) core has highest CFC-11 concentrations along 28°N within 300 km of the boundary (Fig. 8, lower panel). The deep core has highest concentrations even closer to the boundary in a narrow (<100 km) core, with a maximum value at cast 67 near 3400 m that is significantly higher than observed anywhere in the deep core along the 29°–30°N section. This poses an interpretative dilemma as to how it is possible for the higher F11 concentrations to reach 28°N without passing through the 29°N section. This puzzle may be an artifact of the sampling resolution. Along 29°N the 25 n mi station spacing was such that successive bottom depths were 3200 and 5100 m. It may be that the DWBC becomes quite narrow at this location due to the steep continental slope and the station spacing did not adequately resolve the tracer maximum along 29°N at the western boundary. There is also undoubtedly a certain amount of inherent ''patchiness'' in the tracer distributions. Farther offshore, over the western flank of the Bahama Ridge (CTD stations 63, 62) there is a second patch of higher CFC-11 concentrations in the deep layer, probably due to deep recirculating flow over the Bahama Ridge, as will be described in the following section.

The 26.5°N transect crosses the steep slope of the Blake Escarpment, runs up and over the Bahama Ridge, and into the deeper waters over the Hatteras Abyssal Plain out to 71°W (Fig. 9, upper panel). The velocity section (Fig. 9, middle panel) shows the high southward velocity core of the DWBC located somewhat farther offshore (100 km) than is usually observed along this well-studied section (Lee et al. 1990; Leaman and Harris 1990; Lee et al. 1996). The southward core is separated from the boundary by a narrow band of northward flow. Lee et al. (1996) have frequently observed northward flow along the boundary when the DWBC axis meanders offshore. The southward velocity maximum is at mid depth (about 2000 m), located adjacent to a similar middepth maximum of northward flow over the Bahama Ridge. Weaker, broad southward deep flow is found over the entire offshore half of the transect out to 71°W.

In the 4°–6°C layer along 26.5°N, the highest CFC-11 concentrations are located close to the boundary inshore of the velocity core, but relatively high concentrations also extend quite far to the east to at least 300 km (Fig. 9, lower panel). Within the deeper 1.9°–2.4°C layer at 26.5°N, CFC-11 concentrations reach a maximum similar to or even higher than those at 28°N (Fig. 8). High CFC-11 concentrations (>0.30 pmol kg^{-1}) extend out from the boundary to about 180 km. Yet relatively high CFC-11 concentrations (>0.20 pmol kg^{-1}) extend all the way out to the eastern limit of the study area (station 15). This is in marked contrast to the CFC-11 distribution along the 29°–30°N section (Fig. 7), where the 0.20 pmol kg^{-1} contour is narrowly confined to the

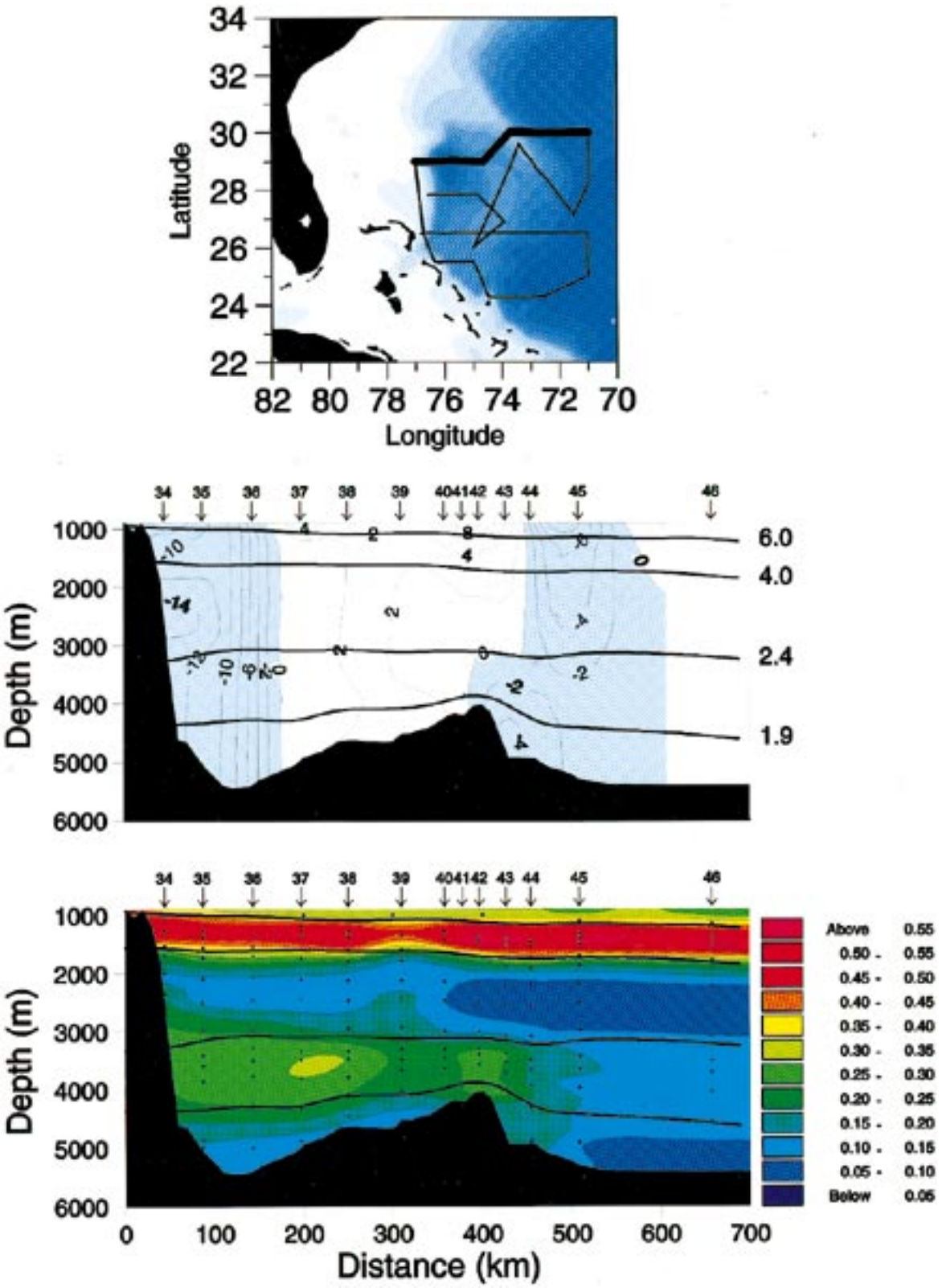

FIG. 7. Upper panel: Cruise track superimposed on bottom topography contours. Location of the 29°–30°N transect is indicated by bold line segment. Middle panel: Referenced geostrophic velocity (in cm s^{-1}) along 29°–30°N (velocity component shown is perpendicular to station pairs; positive is northward for east–west transect heading). Lower panel: CFC-11 (in pmol kg^{-1}) along 29°–30°N. Selected contours of potential temperature (6°, 4°, 2.4°, and 1.9°C) are superimposed on velocity and CFC-11 sections.

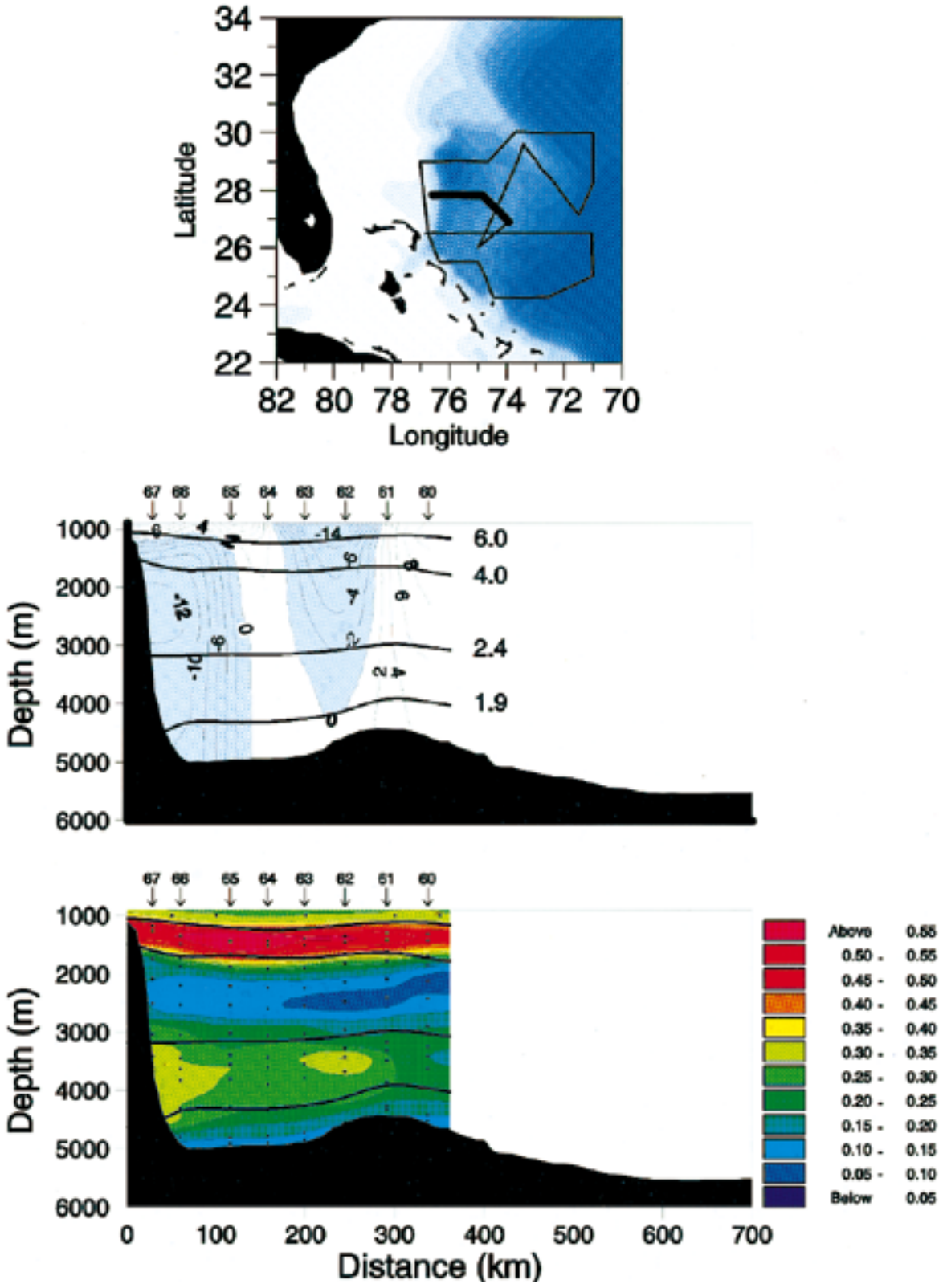

FIG. 8. Same as Fig. 7 but for the 28°N section.

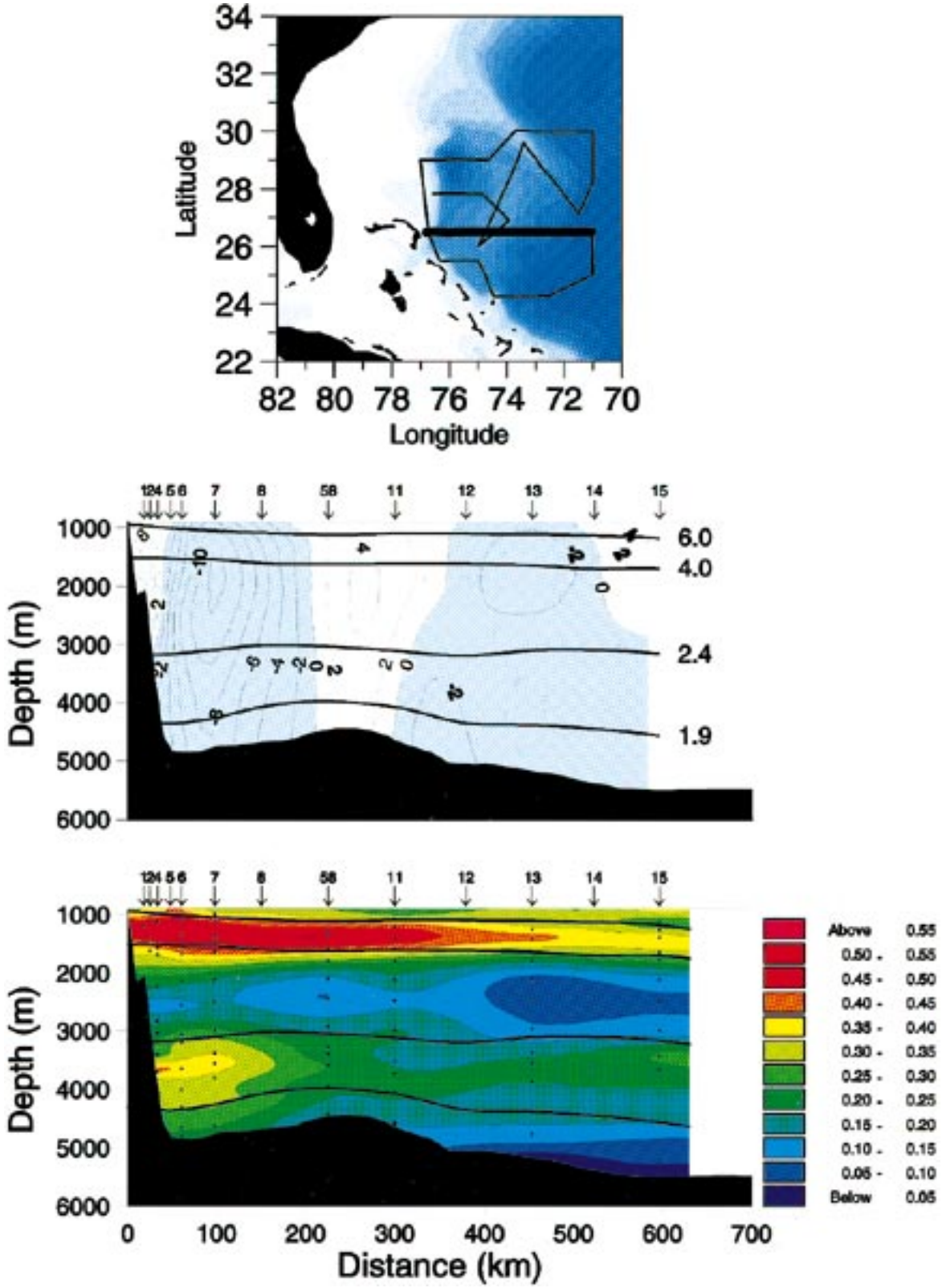

FIG. 9. Same as Fig. 7 but for the 26.5°N section.

4800-m isobath just east of the BBOR crest (stations 43, 44).

The southernmost transect crosses the Blake Escarpment at 25.5°N, runs out to the Bahama Ridge at 75°W, angles southward to the San Salvador Spur just north of 24°N, and then eastward out to 71°W over the Hatteras Abyssal Plain (Fig. 10, upper panel). Thus, this section crosses the DWBC three times as the section ''doglegs.'' The velocity field (Fig. 10, middle panel) shows that the DWBC follows the bottom topography, flowing southward at 25.5°N (stations 31–28), eastward (stations 28–26), and finally southward again at 24°N (stations 25–21) having passed the San Salvador Spur. The vertical structure of the DWBC flow is very similar to that of the other transects, with a persistent middepth current core at about 1800-m depth. This changes by the time the flow reaches 24°N, where there is now evidence of a deeper current maximum, that is, a tendency toward bottom intensification of the current structure.

The CFC-11 concentrations in the two DWBC cores, although quite limited in sampling resolution along this section, show relatively high values extending southward along the boundary past 24°N (Fig. 10, lower panel). These patterns will be shown more clearly in the map portrayals of the following section.

5. Horizontal maps

Flow pathways and transport magnitudes of the various layers can be examined further using a combination of horizontal maps of transport within selected potential temperature layers and CFC-11 concentrations on selected potential temperature surfaces within the layers. Salinity is included for the uppermost layer, where it provides useful additional information. These maps (Figs. 11–18) show strong correlations between bottom topography and tracer properties for the waters below 6°C. In general, as was shown in the vertical sections, the highest deep equatorward velocities and most recently ventilated waters are found along the western boundary and to a lesser extent on the crest of the BBOR. In plan-view the cyclonic recirculation gyres located just to the east of the equatorward western boundary current are now clearly evident. It should be noted that the transport vector maps represent direct observations of the flow field only along the 26.5°N section and elsewhere are based upon the referencing methodology described in section 3. Finally, as with mapping any observed tracer fields, there may be alternate ways to draw the various contours, particularly in the vicinity of the recirculation gyres.

A transport streamline map for the total flow at potential temperatures less than 6°C is shown in Fig. 11. Approximately 11 Sv flows around the BBOR and turns westward at 29°–30°N to join 20 Sv that have taken a more direct southward route along the continental slope north of the study area. The combined 31 Sv continues along the boundary and flows equatorward past the San Salvador Spur at 24°N. An additional 12 Sv forms a large recirculation gyre between 75.5° and 74°W, with a north–south extent from 25° to 29.5°N of about 500 km. Embedded within this gyre are two smaller closed cyclonic subgyres, one containing 4 Sv located over the deep water of the Blake Basin, and the other containing 8 Sv centered just south of the 26.5°N transect at 75°W. Farther offshore, additional southward flow adds 16 Sv for a total deep equatorward transport of 47 Sv at 24°N.

The transport map for the shallowest layer, 4°–6°C (Fig. 12), is generally similar to the total transport streamlines, with a few exceptions. The flow streamlines are more zonally oriented, flowing westward across the BBOR at 30°N, and there is a small anticyclonic eddy located at the eastern end of the 26.5°N transect. In this layer 3 Sv flows westward across the BBOR to join 2 Sv of western boundary flow from the north. The offshore southward flow component adds 4 Sv to the 5-Sv boundary flow at 24°N for a total of 9 Sv. The narrow equatorward western boundary flow at 29°, 28°, and 26.5°N has high CFC-11 concentrations (Fig. 13a) and relatively low salinities (Fig. 13b). Within the cyclonic gyres CFC-11 concentrations are generally also high but patchy, suggesting a complicated mixing zone tending toward homogenization as might be expected for a recirculation regime. The highest CFC-11 concentrations in this layer are found at and offshore of the BBOR along 30°N. However, the salinity of the high CFC-11 water along 30°N east of the BBOR crest is considerably higher ($>$35.022 psu) than the salinity of the narrow western boundary flow ($<$35.018 psu). This difference in salinity suggests that the westernmost, fresher boundary flow comes into the area at 29°N from the north and completely bypasses the BBOR, whereas the high CFC-11, higher salinity water at and offshore of the BBOR is from a different source. The lowest CFC-11 concentrations and highest salinities within this temperature layer are associated with an anticyclonic eddy near 26.5°N, 71°W (the most striking tracer anomaly on the 4.4°C surface), and also in the southeastern corner of the study area. The origin of these higher salinities will be discussed in the following section.

The transport streamlines of the middle layer, 2.4°–4.0°C (Fig. 14), associated with the CFC-11 minimum, are qualitatively similar to the upper layer (Fig. 12), except that the magnitudes of the transports are considerably higher indicative of its increased thickness and higher speeds (Figs. 7–10, middle panel). Approximately 4 Sv flows around the BBOR to join 10 Sv flowing south along the boundary, for a sum of 14 Sv which exits the study area at 24°N adjacent to the coastline. The transport of the larger recirculation gyre is 6 Sv, with a smaller gyre containing an additional 5 Sv embedded within it just south of the 26.5°N section. Southward offshore flow adds an additional 7 Sv for a total equatorward flow of 21 Sv at 24°N in this layer. Lowest CFC-11 concentrations are again found offshore

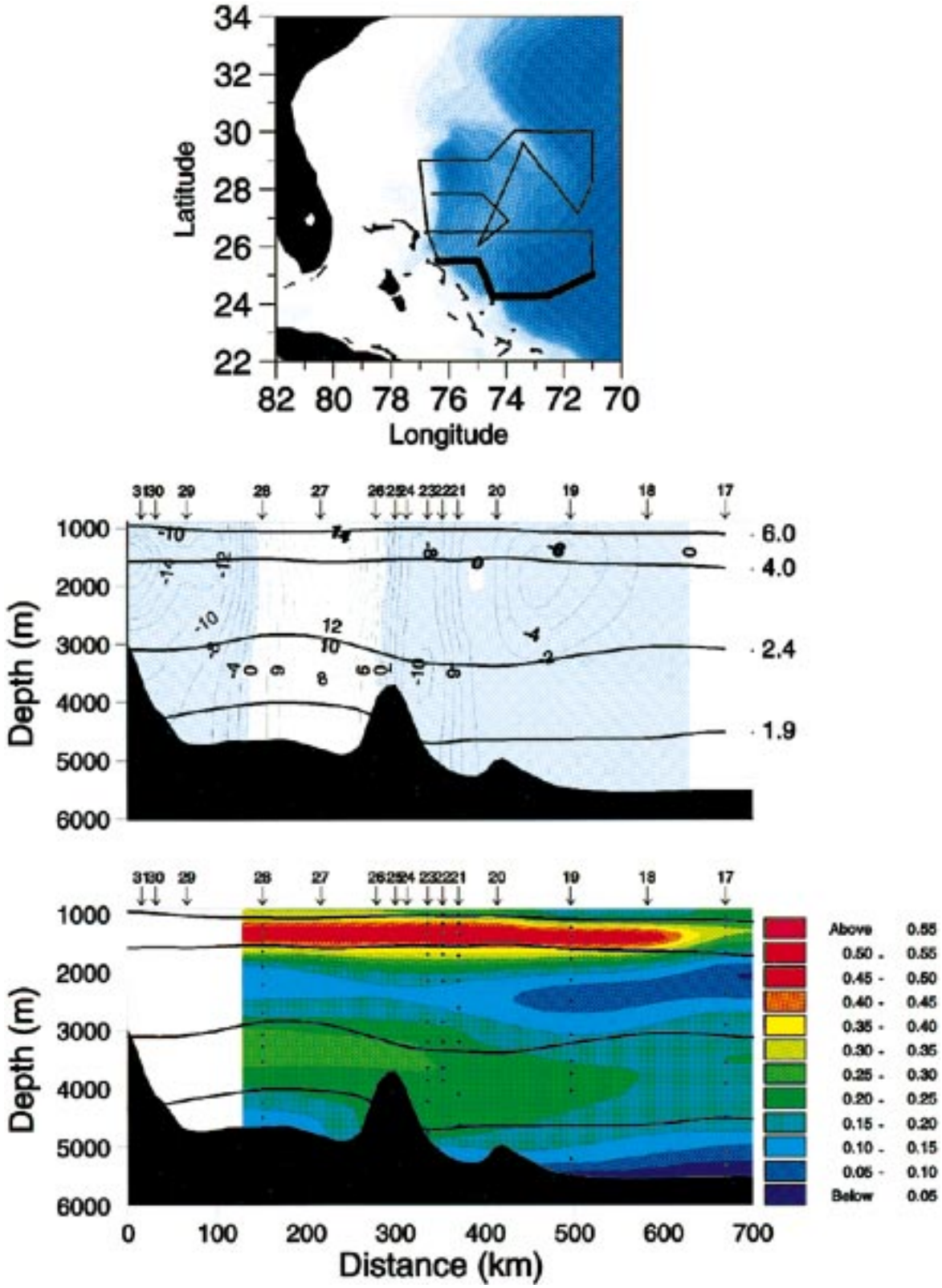

FIG. 10. Same as Fig. 7 but for the 25.5°–24°N section.

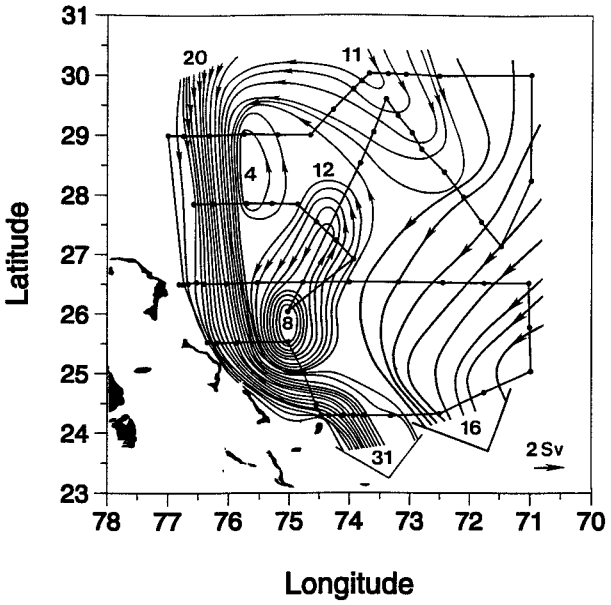

FIG. 11. Transport schematic (one streamline = 2 Sv) for total deep flow (below a potential temperature of 6°C).

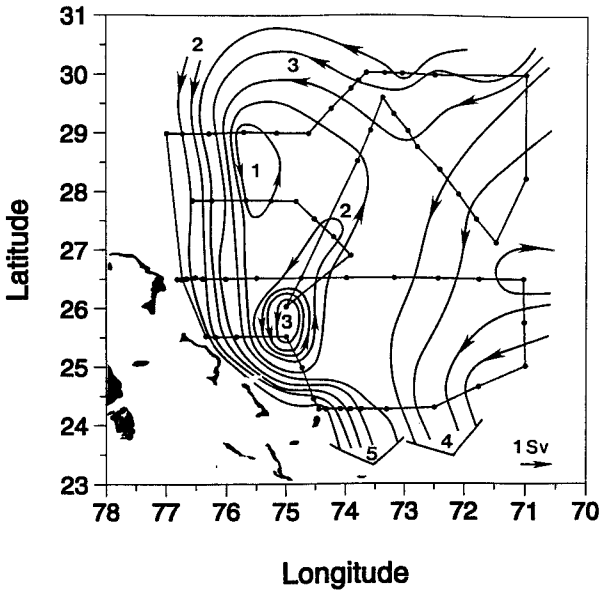

FIG. 12. Transport schematic (one streamline = 1 Sv) for the 4°–6°C potential temperature layer.

of the recirculation gyres (Fig. 15a). All of the values east of 73.5°W, including those located on the BBOR, are less than 0.10 pmol kg^{-1}. The recirculation gyre has intermediate concentrations of CFC-11. A very narrow band of high CFC-11 (>0.16 pmol kg^{-1}) concentrations is found adjacent to the continental slope, extending equatorward from 30° to at least 24°N. Some of this higher CFC-11 water also appears to be steered northeastward following the topography of the southern extension of the Bahama Ridge, extending northward along 74°W to 27°N with the northward flow of the recirculation gyre (Fig. 14).

The transport streamlines for the deep core, 1.9°–2.4°C (Fig. 16), are also similar to the other layers except that the recirculation over the Bahama Ridge is narrower and the small cyclonic gyre south of 26.5°N is no longer a separate feature. There are 7 Sv transported equatorward along the boundary, joined by 2 Sv from the crest of the BBOR, with the offshore flow component adding an additional 3 Sv for a total equatorward flow of 12 Sv at 24°N. The CFC-11 concentrations (Fig. 15b) suggest that the most recently ventilated water follows the isobaths by turning westward toward the boundary before reaching the tip of the BBOR, with older, less ventilated water present over much of the BBOR and offshore regions. Highest CFC-11 concentrations are found along the western boundary and clearly extend into the northern recirculation gyre. Concentrations in general tend to decrease markedly in the equatorward as well as in the offshore direction. As discussed above, due to sampling resolution the tracer maximum may have been missed at 29°N since the CFC-11 maximum is found at 26.5°N. However, as the 26.5°N transect was occupied earlier than the other more northern transects, this may simply be a manifestation of temporal variability of the mapped tracer field and/or lack of synopticity of the observations. Note that, in contrast to the more zonally oriented CFC-11 distribution of the shallow core, in this deeper layer the highest CFC-11 concentrations are all located along the boundary in the western half of the study area, and the lowest CFC-11 concentrations are found in the northeast corner of the study region.

The flow of bottom waters (<1.9°C; Fig. 17) is strongly correlated with the bottom topography. In this bottom layer, 2 Sv of the most recently ventilated water flows around the BBOR, then turns back westward to join an additional 1 Sv and flow equatorward along the western boundary for a total flow along the boundary of 3 Sv. The cyclonic recirculation gyre carries 1 Sv more. Another 2 Sv join the southward flow from offshore of 74°W for a total of 5 Sv of equatorward boundary flow colder than 1.9°C exiting the region at 24°N. In this deepest layer, the highest CFC-11 concentrations are found at the BBOR and not along the western boundary (Fig. 18a), and extend farther to the southeast along the BBOR axis than in the other layers. It appears that, only in this bottom layer, the relatively highest CFC-11 concentrations flow southeastward out along the eastern

→

FIG. 13. (a) CFC-11 concentration (pmol kg^{-1}) on the 4.4°C potential temperature surface. (b) Salinity on the 4.4°C potential temperature surface.-

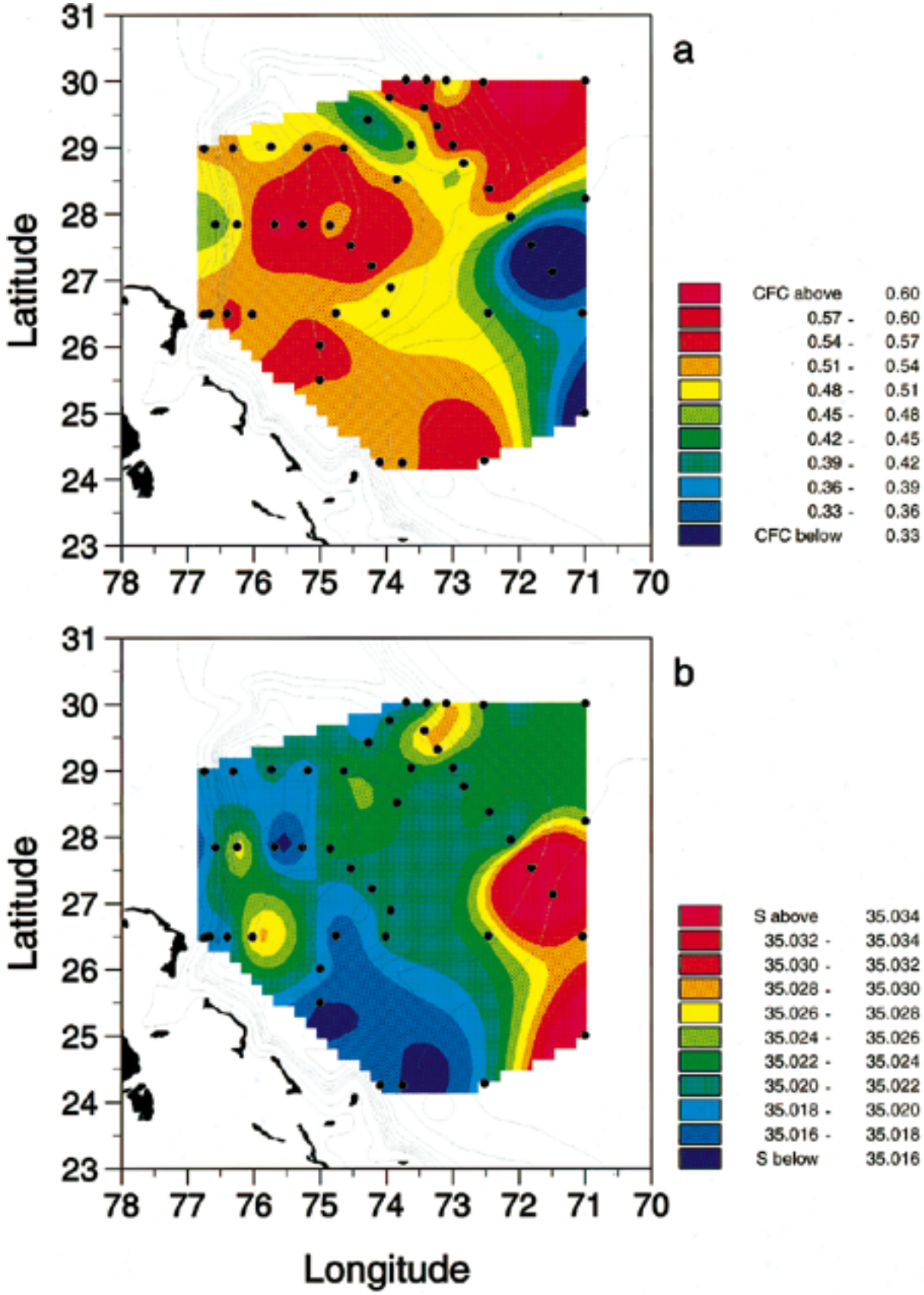
a
b
Latitude
Longitude
31
30
29
28
27
26
25
24
23
78
77
76
75
74
73
72
71
70
CFC above 0.60
0.57 - 0.60
0.54 - 0.57
0.51 - 0.54
0.48 - 0.51
0.45 - 0.48
0.42 - 0.45
0.39 - 0.42
0.36 - 0.39
0.33 - 0.36
CFC below 0.33
S above 35.034
35.032 - 35.034
35.030 - 35.032
35.028 - 35.030
35.026 - 35.028
35.024 - 35.026
35.022 - 35.024
35.020 - 35.022
35.018 - 35.020
35.016 - 35.018
S below 35.016

flank of the BBOR following the isobaths to the ridge crest near 28°N before turning back around to the north, as was suggested by Amos et al. (1971). The CFC-11 concentrations are relatively high all along the boundary, although not quite as high as those at the BBOR. The lowest CFC-11 concentrations, located along the eastern part of the study area, are coincident with the coldest bottom temperatures (Fig. 18b) and lowest bottom salinities (not shown), and are associated with remnants of Antarctic Bottom Water.

6. Discussion

a. Large-scale current pathways and bottom topography

The coincidence of the tracer distributions and the isobaths suggests that the prominent topographic features in this region strongly influence the circulation, particularly in the deepest layers. At the northern part of the study region, the flow follows the isobaths northwestward around the eastern rim of the Blake Basin, in agreement with earlier work (Tucholke et al. 1973; Amos et al. 1971; Riser et al. 1978). However, it appears that most of the recently ventilated water passes along the boundary north of the BBOR, and only in the coldest layer (<1.9°C) are the highest CFC-11 concentrations observed at the BBOR. The warmer layers apparently turn back northwestward into the boundary, following the shallower isobaths north of the study area before reaching the southern tip of the BBOR. There, due to the steep topography of the Blake Escarpment just west of the Blake Basin, the flow is channeled back into a narrow equatorward boundary flow.

While it appears that the BBOR eventually channels the DWBC flow into the western boundary, the topographic contours at the southern extension of the Bahama Ridge appear to have the opposite effect of deflecting it away from the boundary. Over the Blake Basin and the Bahama Ridge, the transport streamlines and tracer distributions depict a cyclonic gyre with one or more embedded gyres within the larger-scale equatorward boundary flow. Recirculation gyres adjacent to the DWBC have also been observed at other locations (e.g. Hogg 1983; McCartney 1992; Johns et al. 1993). The presence of a seemingly permanent recirculation gyre over the Bahama Ridge contributed to previous reports of larger than expected equatorward transport near the western boundary at 26.5°N (Lee et al. 1990; Molinari 1989; Leaman and Harris 1990).

This northward deflection of part of the recently ventilated deep flow at the southern extent of the Bahama Ridge near 25°N is consistent with two of the floats discussed by Riser et al. (1978). More recent results from another Lagrangian float program conducted in the region (Leaman and Vertes 1996) show the role of the San Salvador Spur in steering the deep flow. Floats passing closest to the spur tend to continue equatorward,

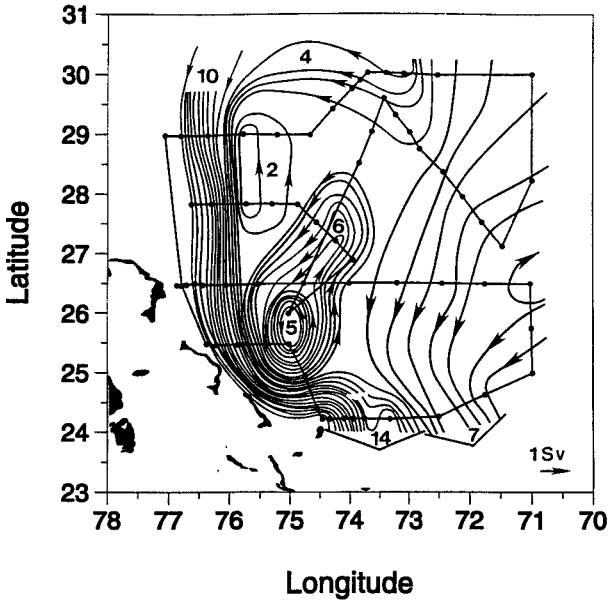

FIG. 14. Transport schematic (one streamline = 1 Sv) for the 2.4°–4°C potential temperature layer.

while those traveling only a small distance farther offshore tend to recirculate to the north. The float trajectories are generally in agreement with the transport maps and the tracer fields observed during June–July 1990. However, this is a very energetic region and the float tracks are complex, dominated by eddies and indicating enhanced local mixing in the area. Few if any floats passed smoothly equatorward past the San Salvador Spur, suggesting that the transport streamlines shown in Figs. 11, 12, 14, 16, and 17 may be somewhat simplistic (or perhaps more representative of the mean flow than any instantaneous Lagrangian realization could be). The paths of two RAFOS floats, which were in the study area during the June–July 1990 hydrographic survey (Vertes and Leaman 1994), are of particular interest. These two floats executed a tight cyclonic eddy movement just south of the 26.5°N transect between 76° and 74°W, agreeing remarkably well with the closed geostrophic transport streamlines in the small embedded eddy of 8 Sv (Fig. 12), confined between the 25.5° and 26.5°N transects, demonstrating the consistency between the Lagrangian and geostrophic representations of the synoptic flow.

Notwithstanding the recirculation gyres, 31 Sv of more recently ventilated deep flow makes its way equatorward adjacent to the continental slope past 24°N (Fig. 11) and out of the study area, joined at 24°–25°N by an additional 16 Sv of less recently ventilated water for a total equatorial transport of 47 Sv at 24°N. Based on other observations (Fine and Molinari 1988; Molinari et al. 1992; Weiss et al. 1985; Speer and McCartney 1991; Friedrichs et al. 1994; Wallace et al. 1994; Rhein et al. 1995), it is known that the DWBC continues southeastward along the Bahamian Island Chain past the is-

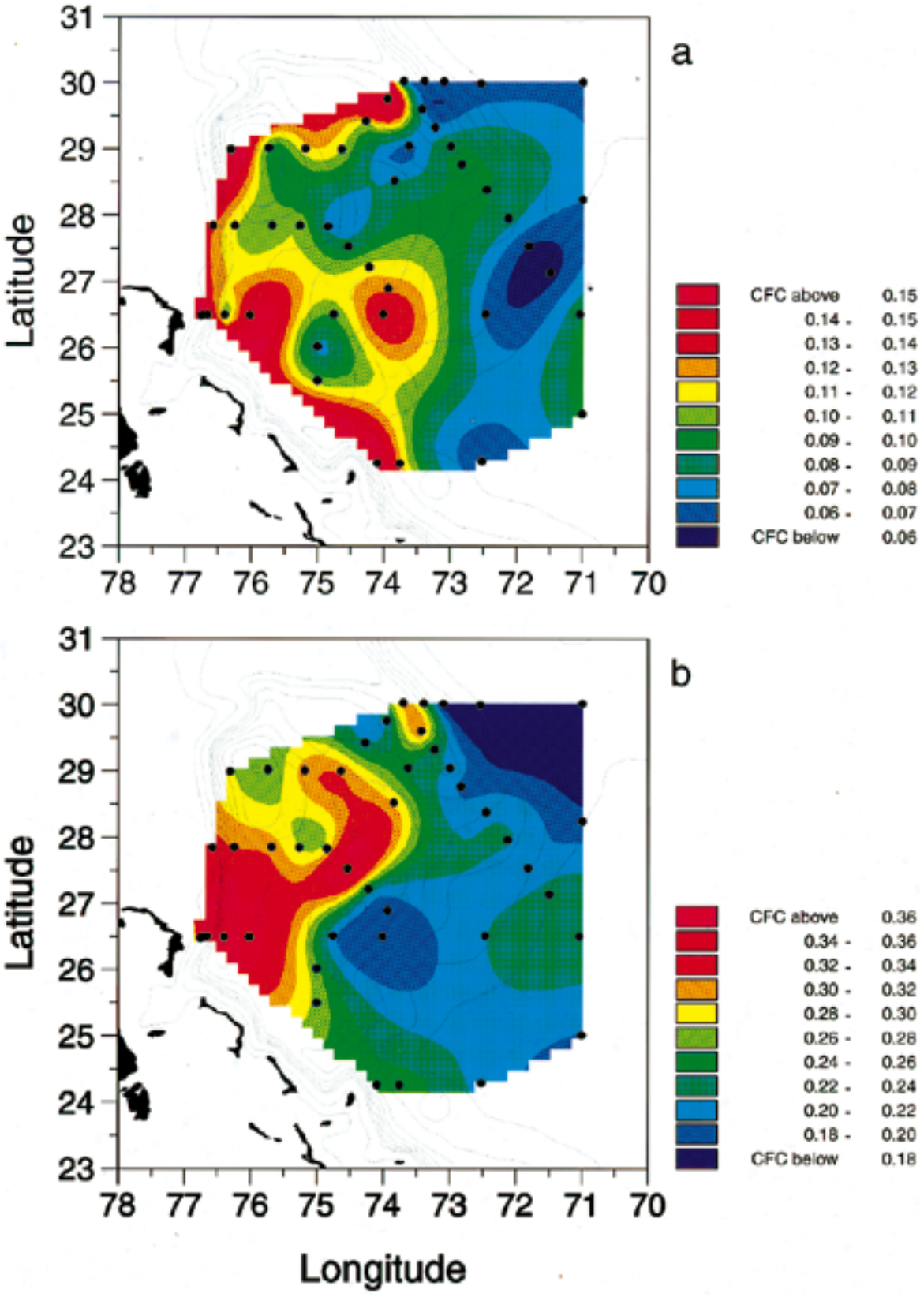

FIG. 15. CFC-11 concentration (pmol kg^{-1}) on (a) the 3.0°C and (b) the 2.1°C potential temperature surface.

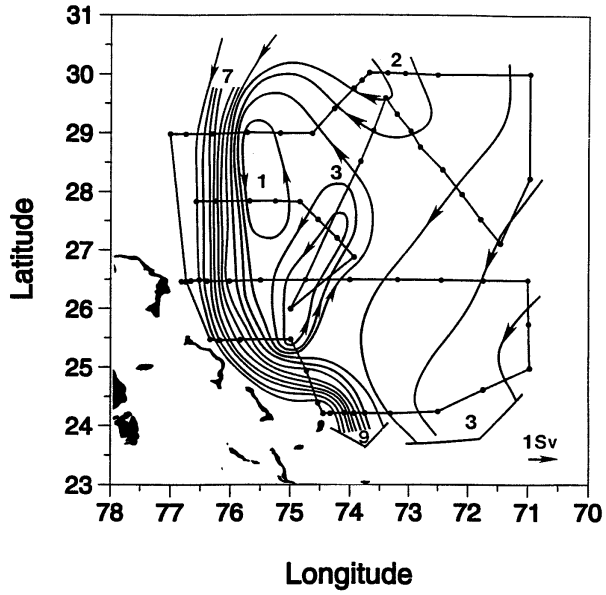

FIG. 16. Transport schematic (one streamline = 1 Sv) for the 1.9°–2.4°C potential temperature layer.

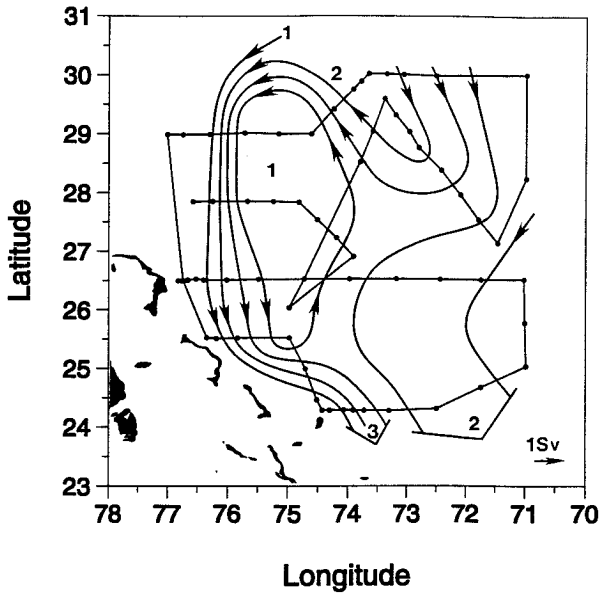

FIG. 17. Transport schematic (one streamline = 1 Sv) for the <1.9°C potential temperature layer.

lands of the eastern Caribbean and into the Southern Hemisphere, although there are further recirculations and diversions of the flow along the way (for example, in the Guiana Basin at 7°N: Johns et al. 1993; McCartney 1992).

b. *Influence of the Gulf Stream on flow pathways and tracer concentrations*

Bottom topography appears to have less of an influence on the shallowest (4° to 6°C) temperature layer in the June–July 1990 data. Both the circulation and the tracer characteristics of this shallow layer are different from the deeper layers. At the level of the shallow core, 2 Sv of the most recently ventilated, lowest salinity water enter the study area along the boundary from the north, having bypassed the BBOR, and continue equatorward along the western boundary (Figs. 12, 13). However, there are also 3 Sv carried westward across the axis of the BBOR with CFC-11 concentrations even higher than those in the branch of the DWBC flowing southward along the Blake Escarpment. These high CFC-11 concentrations to the east, over the BBOR, are associated with significantly higher salinity than found in the boundary flow, suggesting that the westward zonal flow originates from a different source region.

This offshore, high CFC-11/high salinity water mass can be traced to the southern side of the Gulf Stream recirculation gyre (Worthington 1976; Schmitz and McCartney 1993). Just north of the Gulf Stream crossover, as shown by Pickart and Smethie (1993), the upper part of the shallow CFC core carried by the DWBC (at densities corresponding to 5° to 8°C) does not pass underneath the Gulf Stream but rather recirculates completely into the interior north of the Gulf Stream. However, the lower part (4° to 5°C) does both: part of it is carried offshore and, also, some portion crosses under the Gulf Stream and continues equatorward along the steep part of the continental slope, eventually forming the narrow boundary current found along the Blake Escarpment in the June–July 1990 study area. Our data suggest that the branch of current containing the high CFC core, which has been carried offshore, having traveled by a less direct route involving one or more transits around the Gulf Stream recirculation gyre, finally rejoins the western boundary at and offshore of the BBOR at 30°N. This water mass retains much of its recently ventilated characteristics, that is, elevated concentrations of CFC-11, but also acquires a higher salinity signal along the way due to interaction with the Mediterranean Water in the eastern subtropical Atlantic as described in Reid (1994). The higher salinity, low CFC-11 features observed in the southeastern part of the study area (Figs. 13a,b), on the other hand, also likely originate in the region of Mediterranean Water influence, not from recently ventilated but rather ''older'' intermediate waters south of the Gulf Stream recirculation.

c. *Ventilation of the interior and equatorward dilution of the DWBC tracer concentrations*

The cyclonic recirculation gyres between the BBOR and the San Salvador Spur are one of the more striking features of the regional deep flow. Although they may have only a regional effect on the circulation, nevertheless they serve to ventilate the interior and dilute the tracer concentration carried equatorward by the DWBC. One consequence of the recirculation gyres is that there

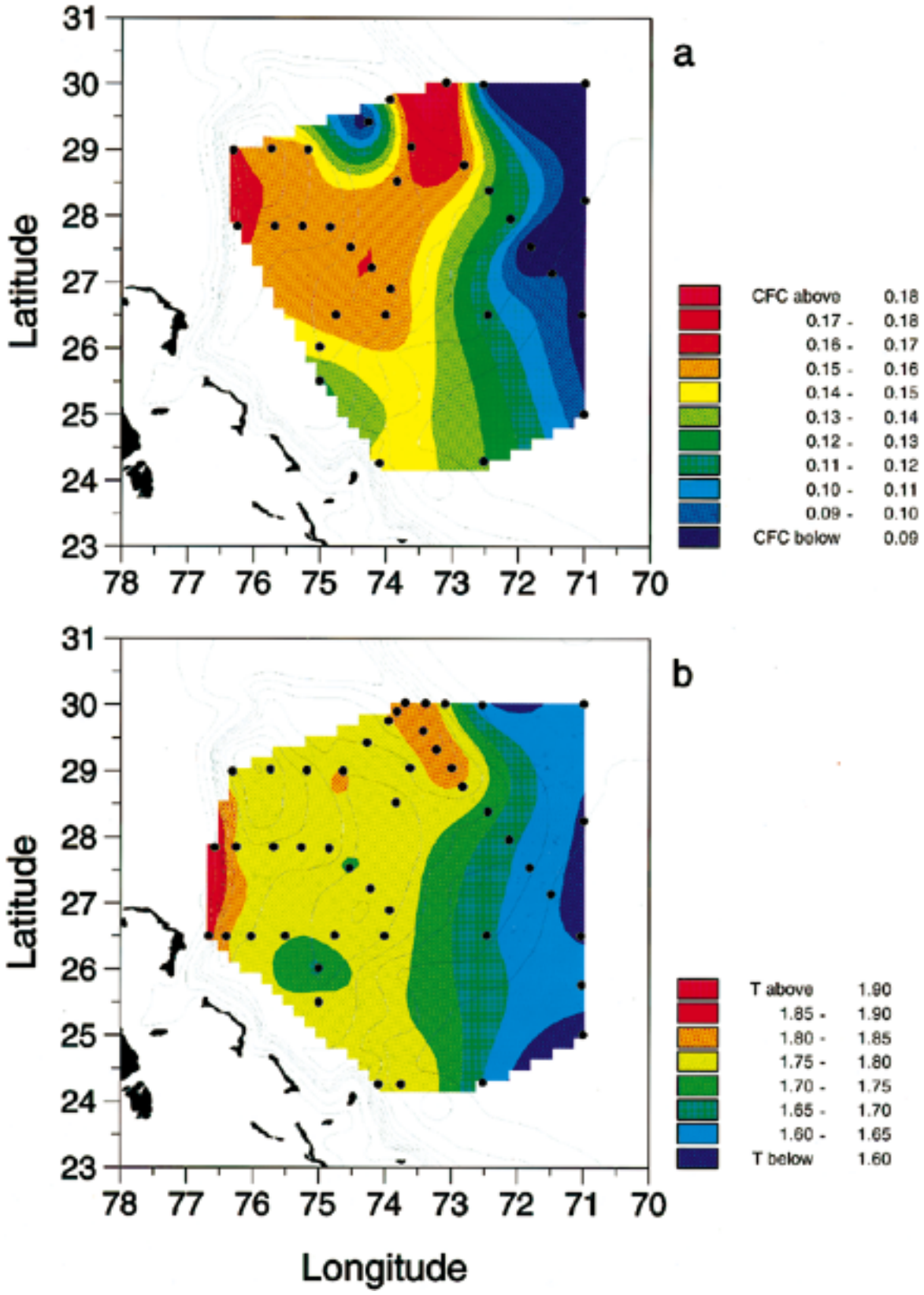

FIG. 18. CFC-11 concentration (pmol kg^{-1}) on the 1.8°C potential temperature surface (a) and potential temperature (°C) at the bottom (b).

are fairly high concentrations of CFCs extending offshore at 26.5°N, indicating that the region east of Abaco may be acting to mix or diffuse the tracer fields of the DWBC. For example, the horizontal CFC-11 gradient in the deep core (on the 2.1°C surface, Fig. 15b) is very sharp at 30°N over the crest of the BBOR, where concentrations decrease from a maximum of >0.30 pmol kg^{-1} to less than 0.18 pmol kg^{-1} in a horizontal distance of only 50 km. In contrast, at 26.5°N the CFC-11 gradient has become much more diffuse, and almost all values out to at least 71°W, more than 600 km from the boundary, are greater than 0.20 pmol kg^{-1}. The CFC-11 gradient remains diffuse south of 26.5°N. This pattern seems to indicate ''ventilation'' due to diffusion or mixing along the edges of the deep currents, where the horizontal shears are greatest, or advection into the interior followed by mixing, which is intensified at the latitudes of the recirculation gyres. The float tracks of Leaman and Vertes (1996) also indicate enhanced advective and/or diffusive mixing in the local region, as discussed above. The net effect is that DWBC recirculation gyres, and enhanced mixing due to topographic influences, appear to be an effective means for ventilation of the interior and dilution of the DWBC tracer concentrations.

d. Offshore deep flow

The broad, southward offshore flow carrying low CFC water is observed throughout the study region east of 74°W. Bottom photographic data compiled by Tucholke et al. (1973) also show deep flow to the south in the same area (25° to 27°N, 72° to 73°W). Furthermore, recent direct velocity observations made using a lowered acoustic Doppler current profiler during August 1992 show southward deep flow of about 5 cm s^{-1} below 1000 m, present along 26.5°N from the eastern edge of the recirculation gyre out to 71°W (Hacker et al. 1996). This circulation pattern could be linked to the Schmitz and McCartney (1993) portrayal of an elongated recirculation gyre located just offshore of the DWBC between 1.8° and 4.0°C, which extends from the Guiana Basin near the equator to 30°N in the western North Atlantic, adding an additional 17 Sv of southward flow to the DWBC south of 30°N. The transport magnitude is consistent with the June–July 1990 data, from which it is estimated that offshore of the 31 Sv component that flows adjacent to the steep continental slope, an additional 16 Sv are transported equatorward through the study region. The June–July 1990 transport data (Fig. 11) provide a suggestion of the northern limit of the large-scale recirculation gyre of Schmitz and McCartney (1993).

In contrast, the Leaman and Vertes (1996) float tracks clearly show flow to the north at all three depth levels (1250 m, 2000 m, and 3500 m) in the same offshore region. However, most of these floats were launched after 1991. This suggests that the large-scale deep flow in the offshore study region is temporally variable, with periods of northward as well as southward flow, and that the results reported herein for June–July 1990 may not necessarily represent mean conditions. However, the float observations do not rule out the existence of the mean elongated gyre of Schmitz and McCartney (1993) described above. It is possible that this gyre varies in its northernmost limit, extending for example to almost 30°N during 1990 but shrinking back to south of 25°N during the RAFOS float program in 1991 to 1993. Long-term direct current measurements, either from current meter arrays or large ensembles of floats, will probably be necessary to determine the mean large-scale deep flow.

7. Summary

South of the BBOR the tracers and transports show a complex pathway for the DWBC, which includes recirculation gyres with spatial scales ranging from a few hundred kilometers to nearly basin scale. The flow is dominated by the branch immediately adjacent to the western boundary, which carries two distinct cores of high CFC-11 indicating relatively recent ventilation, in a narrow, strong boundary current. This boundary current is joined from offshore at 24°N by an additional lower CFC-11 equatorward flow of 16 Sv. Thus, the total transport below 6°C at 24°N is 47 Sv for the June–July 1990 period, of which 31 Sv are the most recently ventilated component of the DWBC, which flows southward close to the boundary along the Blake Escarpment.

The close correspondence of the tracer distributions with the regional topography indicates that the major topographic features in this region strongly influence the circulation, particularly in the deep and bottom layers. In the northern part of the study region, the near-bottom flow follows the isobaths around the BBOR and northwestward along the eastern rim of the Blake Basin, in agreement with earlier work (Tucholke et al. 1973; Amos et al. 1971; Riser et al. 1978). However, it appears that the most recently ventilated water at slightly shallower depths bypasses the BBOR to the north, and only in the coldest layer (<1.9°C) are the highest CFC-11 concentrations observed at the BBOR. South of the BBOR, the more recently ventilated component of the DWBC is channeled into a narrow equatorward flow due to the steep topography along the Blake Escarpment west of the Blake Basin. At the southern part of the study region (24°N), some of the more recently ventilated water appears to be steered northward around the extension of the Bahama Ridge.

Both the circulation and ventilation characteristics of the shallow (4°–6°C) layer are different from the deeper layers. In the shallow layer, the flow in the DWBC along the boundary is approximately 2 Sv, with an additional 3 Sv carried westward across the axis of the BBOR from east to west. This offshore flow component on the BBOR, having high CFC-11 and high salinity, can be

traced to the Gulf Stream recirculation gyre (Worthington 1976; Schmitz and McCartney 1993) and is consistent with Pickart and Smethie's (1993) conclusion that a substantial portion of the DWBC water in this depth range is swept into this recirculation gyre at the DWBC/Gulf Stream crossover. The high salinity signal is then gained from interaction with the high salinity Mediterranean Sea water mass to the east (Reid 1994).

Using the tracers and transports, the spatial scales of the recirculation gyres can be defined and their transport quantified. Over the Blake Basin and Bahama Ridge, out to about 74°W, the transport streamlines depict a cyclonic gyre with one or two embedded gyres just offshore of the intense equatorward boundary current. This seemingly permanent recirculation gyre contributes 12 Sv to the transport near the western boundary at 26.5°N, partly explaining the higher than expected transport at this location based on earlier observations, which had more limited offshore extent (Molinari 1989; Lee et al. 1990; Leaman and Harris 1990; Lee et al. 1996). On a larger scale, even farther to the east, the broad southward offshore flow of 16 Sv observed throughout the study region east of 74°W in the June–July 1990 data may be linked to the Guiana Basin gyre as portrayed by Schmitz and McCartney (1993). More detailed analysis of the flow patterns and water masses along the western boundary between 30°N and the equator will be necessary in order to confirm this connection.

Acknowledgments. The authors are grateful to Kevin Sullivan and Ken Casey for the shipboard CFC analyses; Kevin Maillet for the shore-based calibration of the CFC data; Tom Lee and Rainer Zantopp for the current meter data; and the captain and crew of the NOAA R/V *Malcolm Baldrige*. We thank Mike McCartney for many useful discussions during his visits to CIMAS, and Bill Johns and Tom Lee for their insightful comments on the manuscript. We also thank two anonymous reviewers for making comments and suggestions that greatly improved the manuscript. This research was funded in part by NOAA's Atlantic Climate Change Program. R. A. Fine acknowledges the support through CIMAS under NOAA Cooperative Agreements NA37RJ0200 and NA90RAH00075.

REFERENCES

Amos, A. F., A. L. Gordon, and E. D. Schneider, 1971: Water masses and circulation patterns in the region of the Blake–Bahama Outer Ridge. *Deep-Sea Res.,* **18,** 145–165.

Bullister, J. L., and R. F. Weiss, 1988: Determination of CCl_3F and CCl_2F_2 in seawater and air. *Deep-Sea Res.,* **35,** 839–853.

Fine, R. A., 1995: Tracers, time scales, and the thermohaline circulation: The lower limb of the North Atlantic Ocean. U.S. National Report to the IUGG 1991–1994 Quadrennial Report. *Rev. Geophys.,* **33**(Suppl.), 1353–1365.

——, and R. L. Molinari, 1988: A continuous deep western boundary current between Abaco (26.5°N) and Barbados (13°N). *Deep-Sea Res.,* **35,** 1441–1450.

Friedrichs, M. A. M., M. S. McCartney, and M. M. Hall, 1994: Hemispheric asymmetry of deep water transport modes in the western Atlantic. *J. Geophys. Res.,* **99,** 25 165–25 179.

Hacker, P., E. Firing, W. D. Wilson, and R. L. Molinari, 1996: Direct observations of the current structure east of the Bahamas. *Geophys. Res. Lett.,* **23,** 1127–1130.

Heezen, B. C., C. D. Hollister, and W. F. Ruddiman, 1966: Shaping of the continental rise by deep geostrophic contour currents. *Science,* **152,** 502–508.

Hogg, N. G., 1983: A note on the deep circulation of the western North Atlantic: Its nature and causes. *Deep-Sea Res.,* **30,** 945–961.

——, R. S. Pickart, R. M. Hendry, and W. M. Smethie Jr., 1986: The northern recirculation gyre of the Gulf Stream. *Deep-Sea Res.,* **33,** 1139–1165.

Hollister, C. D., and B. C. Heezen, 1972: Geologic effects of ocean bottom currents: Western North Atlantic. *Studies in Physical Oceanography,* A. Gordon, Ed., No. 2, Gordon and Breach Science Publishers, 37–66.

Jenkins, W. J., and P. B. Rhines, 1980: Tritium in the deep North Atlantic Ocean. *Nature,* **286,** 877–880.

Johns, E., and A. M. Wilburn, 1993: Hydrographic observations in the western tropical and subtropical North Atlantic Ocean: Atlantic Climate Change Program (ACCP) and Western Tropical Atlantic Experiment (WESTRAX) during 1990. NOAA Data Rep. ERL AOML-22, 103 pp. [Available from 4301 Rickenbacher Cswy., Miami, FL 33149.]

Johns, W. E., D. M. Fratantoni, and R. J. Zantopp, 1993: Deep western boundary current variability off northeastern Brazil. *Deep-Sea Res.,* **40,** 293–310.

Leaman, K. D., and J. E. Harris, 1990: On the average absolute transport of the deep western boundary current east of Abaco Island, the Bahamas. *J. Phys. Oceanogr.,* **20,** 467–475.

——, and P. S. Vertes, 1996: Topographic influences on recirculation in the deep western boundary current: Results from RAFOS float trajectories between the Blake–Bahama Outer Ridge and the San Salvador ''Gate.'' *J. Phys. Oceanogr.,* **26,** 941–961.

Lee, T. N., W. Johns, F. Schott, and R. Zantopp, 1990: Western boundary current structure and variability east of Abaco, Bahamas, at 26.5°N. *J. Phys. Oceanogr.,* **20,** 446–466.

——, ——, R. Zantopp, and E. Fillenbaum, 1996: Moored observations of western boundary current variability and thermohaline circulation at 26.5°N in the subtropical North Atlantic. *J. Phys. Oceanogr.,* **26,** 962–983.

Livingston, H. D., J. H. Swift, and H. G. Ostlund, 1985: Artificial radionuclide tracer supply to the Denmark Strait overflow water between 1972 and 1981. *J. Geophys. Res.,* **90,** 6971–6982.

McCartney, M. S., 1992: Recirculating components to the deep boundary current of the northern North Atlantic. *Progress in Oceanography,* Vol. 29, Pergamon, 283–383.

——, and L. D. Talley, 1984: Warm-to-cold water conversion in the northern North Atlantic Ocean. *J. Phys. Oceanogr.,* **14,** 922–935.

——, and R. A. Curry, 1993: Transequatorial flow of Antarctic Bottom Water in the western Atlantic Ocean: Abyssal geostrophy at the equator. *J. Phys. Oceanogr.,* **23,** 1264–1276.

Mills, C. A., and P. B. Rhines, 1979: The deep western boundary current at the Blake–Bahama Outer Ridge: Current meter and temperature observations, 1977–78. Woods Hole Oceanographic Institution Tech. Rep. WHOI-79-85, WHOI, Woods Hole, MA, 77 pp.

Molinari, R. L., 1989: Subtropical Atlantic Climate Studies (STACS): An update. *Oceanography,* **2** (2), 32–35.

——, R. A. Fine, and E. Johns, 1992: The deep western boundary current in the tropical North Atlantic Ocean. *Deep-Sea Res.,* **39,** 1967–1984.

Olson, D. B., G. H. Ostlund, and J. Sarmiento, 1986: The western boundary undercurrent off the Bahamas. *J. Phys. Oceanogr.,* **16,** 233–240.

Pickart, R. S., 1992: Water mass components of the North Atlantic

Deep Western Boundary Current. *Deep-Sea Res.*, **39,** 1553–1572.

——, and W. M. Smethie Jr., 1993: How does the deep western boundary current cross the Gulf Stream? *J. Phys. Oceanogr.*, **23,** 2602–2616.

Reid, J. L., 1994: On the total geostrophic circulation of the North Atlantic Ocean: Flow patterns, tracers and transports. *Progress in Oceanography,* Vol. 33, Pergamon, 1–92.

Rhein, M., L. Stramma, and U. Send, 1995: The Atlantic Deep Western Boundary Current: Water masses and transports near the equator. *J. Geophys. Res.*, **100,** 2441–2457.

Riser, S. C., H. Freeland, and H. T. Rossby, 1978: Mesoscale motions near the deep western boundary of the North Atlantic. *Deep-Sea Res.*, **25,** 1179–1191.

Rosenfeld, L., R. L. Molinari, and K. Leaman, 1989: Observed and modeled annual cycle of transport in the Straits of Florida and east of Abaco Island, the Bahamas (26.5°N). *J. Geophys. Res.*, **94,** 4867–4878.

Schmitz, W. J., Jr., and M. S. McCartney, 1993: On the North Atlantic circulation. *Rev. Geophys.*, **31,** 29–49.

Smethie, W. M., Jr., 1993: Tracing the thermohaline circulation in the western North Atlantic using chlorofluorocarbons. *Progress in Oceanography,* Vol. 31, Pergamon, 51–199.

——, and J. H. Swift, 1989: The tritium : krypton-85 age of Denmark Straits overflow water and Gibbs Fracture Zone Water just south of Denmark Strait. *J. Geophys. Res.*, **94,** 8265–8275.

Speer, K. G., and M. S. McCartney, 1991: Tracing lower North Atlantic Deep Water across the equator. *J. Geophys. Res.*, **96,** 20 443–20 448.

Swift, J. H., 1984: The circulation of the Denmark Strait and Iceland–Scotland overflow waters in the North Atlantic. *Deep-Sea Res.*, **31,** 1339–1355.

Talley, L. D., and M. S. McCartney, 1982: Distribution and circulation of Labrador Sea Water. *J. Phys. Oceanogr.*, **12,** 1189–1205.

Tucholke, B. E., W. R. Wright, and C. D. Hollister, 1973: Abyssal circulation over the Greater Antilles Outer Ridge. *Deep-Sea Res.*, **20,** 973–995.

Vertes, P. S., and K. D. Leaman, 1994: Pathways in the Deep Western Boundary Current recirculation south of 30°N. RSMAS Tech. Rep. 94-002, University of Miami, Miami, FL, 100 pp. [Available from RSMAS/UM, 4600 Rickenbacher Cswy., Miami, FL 33149.]

Wallace, D. W. R., P. Beining, and A. Putzka, 1994: Carbon tetrachloride and chlorofluorocarbons in the South Atlantic Ocean, 19°S. *J. Geophys. Res.*, **99,** 7803–7819.

Watts, D. R., 1991: Equatorward currents in temperatures 1.8°–6.0°C on the continental slope in the mid-Atlantic Bight. *Deep Convection and Deep Water Formation in the Oceans,* P. C. Chu and J. C. Gascard, Eds., Elsevier, 183–196.

Weiss, R. F., J. L. Bullister, R. H. Gammon, and M. J. Warner, 1985: Atmospheric chlorofluoromethanes in the deep equatorial Atlantic. *Nature,* **314,** 608–610.

Worthington, L. V., 1976: On the North Atlantic circulation. *Johns Hopkins Oceanographic Studies,* No. 6, 110 pp.